



# A biologically multifunctional PDA-LYS composite coating is fabricated on the surface of magnesium alloy vascular stents to promote endothelialization

Yi Ma<sup>1</sup>, Hao-Jie Guo<sup>1</sup>, Jing-An Li<sup>1</sup>, Yan-Chao Wang<sup>1</sup>, Yi-Fan Zhou<sup>1,a)</sup>

<sup>1</sup>School of Material Science and Engineering & Henan Province Key Laboratory of Advanced Light Alloys, Zhengzhou University, 100 Science Road, Zhengzhou 450001, China

<sup>a)</sup>Address all correspondence to this author. e-mail: Zhouyf@zzu.edu.cn

Received: 3 April 2024; accepted: 23 June 2024; published online: 31 July 2024

Due to their excellent mechanical properties and biodegradability, biodegradable magnesium alloy vascular stents have become a hot topic in current research on vascular stent material. However, the further application of magnesium alloy is limited by its rapid degradation rate and insufficient ability to promote surface endothelialization. This study proposed a strategy of co-depositing a PDA-LYS coating on the surface of magnesium alloy treated with an alkaline pre-heating process. Experimental results demonstrated that the PDA-LYS composite coating significantly improved the corrosion resistance of the magnesium alloy. Furthermore, with the increase in LYS content in the samples, the coating facilitated the adhesion and proliferation of endothelial cells and effectively inhibited the excessive proliferation of pathological smooth muscle cells. In summary, the PDA-LYS composite coating had a positive impact on the biocompatibility of magnesium alloy, which has offered a new approach for surface modification of magnesium alloy vascular materials.

## Introduction

Cardiovascular disease (CVD) has become one of the primary factors impacting human life expectancy in recent years [1]. Since the first successful percutaneous transluminal coronary angioplasty, there has been rapid development of vascular stents in the following decades [2]. Currently, magnesium alloys have become excellent materials for biodegradable stents due to their favorable mechanical properties and biocompatibility [3, 4]. However, although the magnesium alloy stent exhibited reduced inflammation during the postoperative period and can be safely biodegraded by human body, its degradation rate was still too rapid to meet the radial support force necessary for progressive vascular reconstruction [5, 6]. Therefore, the current design of magnesium alloy vascular stent coatings primarily faces challenges related to inadequate corrosion resistance and biocompatibility. Thus, a simple and effective method is needed to solve this problem.

In general, methods to improve the corrosion resistance of alloys include alloying [7], heat treatment [8], and surface modification [9]. However, the high concentration of rare earth

elements in alloy design results in increased costs and limited enhancement of corrosion resistance [7, 10]. Therefore, surface modification may be an effective strategy to improve the corrosion resistance and biocompatibility of magnesium alloys [11]. Traditionally, methods such as alkali-heat treatment [12, 13], fluorination treatment [14], sol-gel method [15, 16], and micro-arc oxidation [17] have been employed to address the issue of insufficient corrosion resistance. Among these options, the hot alkali method stands out due to its excellent corrosion resistance, cost-effectiveness, and simplicity. However, when it comes to vascular stents, the main focus lies in preventing intimal hyperplasia and promoting endothelialization.

Lysine (LYS) has been shown to induce angiogenesis, resist nonspecific protein adsorption, and selectively bind to plasmin in plasma to dissolve blood clots [18]. In particular, LYS has the potential to enhance angiogenesis and promote rapid healing [16]. Nunzia Gallo et al. coated LYS with PLGA (poly(lactico-glycolic acid)) copolymer. Through cellular and molecular studies, they demonstrated that PLGA particles loaded with LYS were non-toxic and biocompatible. They also found that these particles stimulated the expression of pro-angiogenic factors,

such as metalloproteinases, focal adhesion kinases, and various cell growth factors [19]. Li et al. found that the adhesion of dopamine (DA) was related to the adjacent LYS residues. The presence of lysine significantly enhanced the adhesion of DA, and the order of DA and LYS was crucial for this synergistic effect [20].

Therefore, in this study, the composite coating of polydopamine (PDA) combined with the excellent biocompatibility of LYS was prepared and loaded on the surface of magnesium alloy to effectively improve the comprehensive properties of magnesium alloy [21, 22]. This strategy further improved the

biocompatibility of PDA, broadened the application range of PDA, and provided a new perspective for the surface modification of magnesium alloy materials (Fig. 1).

## Results and discussion

### Surface characterization

As shown in Fig. 2, the Mg-Zn-Y-Nd alloy presented a relatively uniform and smooth surface. However, there were more holes and cracks on the surface of the Mg-OH and PDA samples. Interestingly, on the surface of PDA-LYS group samples, the

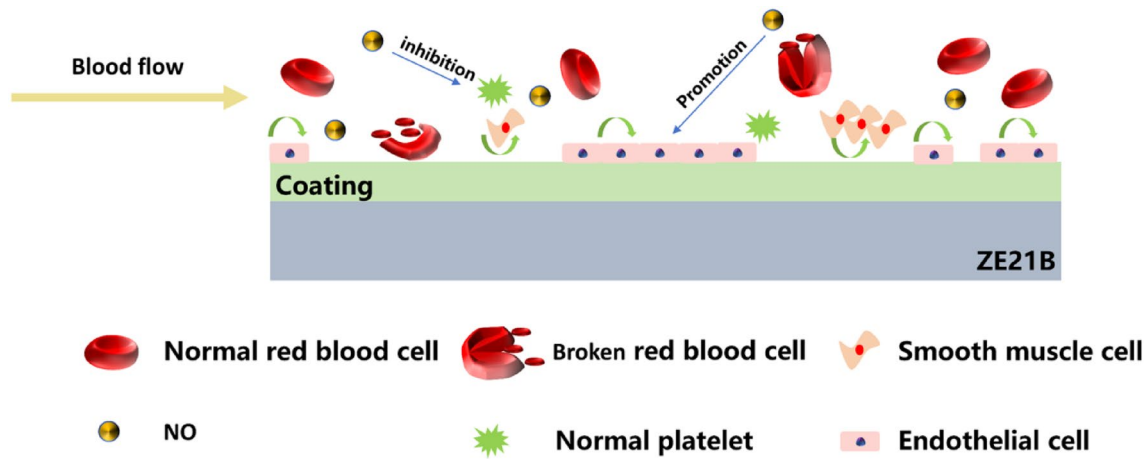


Figure 1: Diagram of the effect of vascular stent implantation in blood vessels.

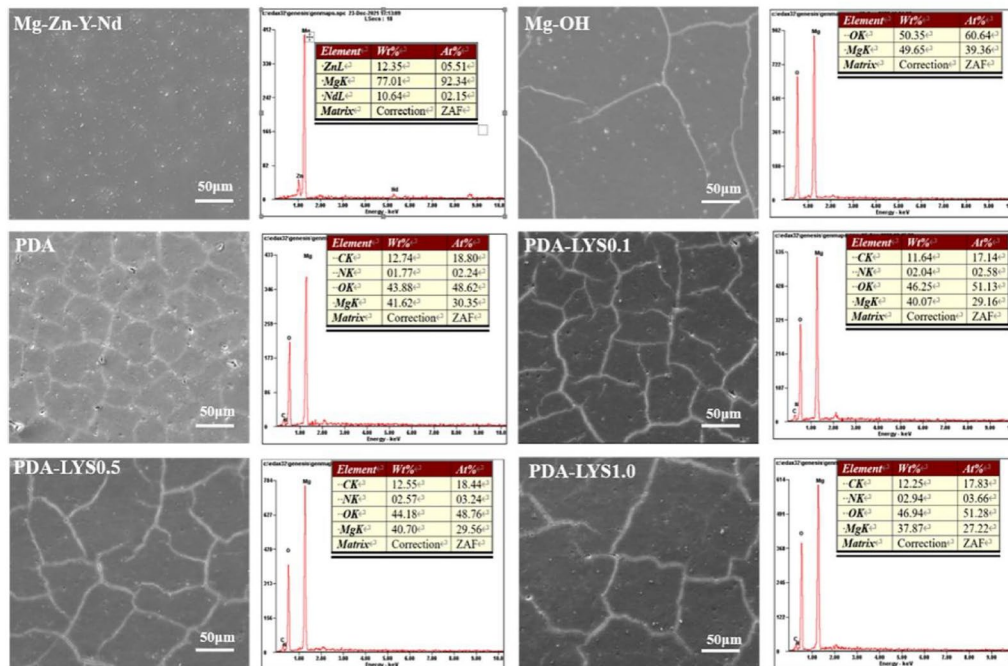


Figure 2: Microtopography and EDS spectra of each sample.

results showed that the cracks on the surface of the PDA-LYS samples were reduced after the addition of three different proportions of LYS, as the LYS content increased, there were fewer cracks and holes on the sample surface, and EDS showed that the coatings were mainly composed of C, N, and O elements. The SEM and EDS results showed that the coating was successfully loaded on the surface of magnesium alloy samples.

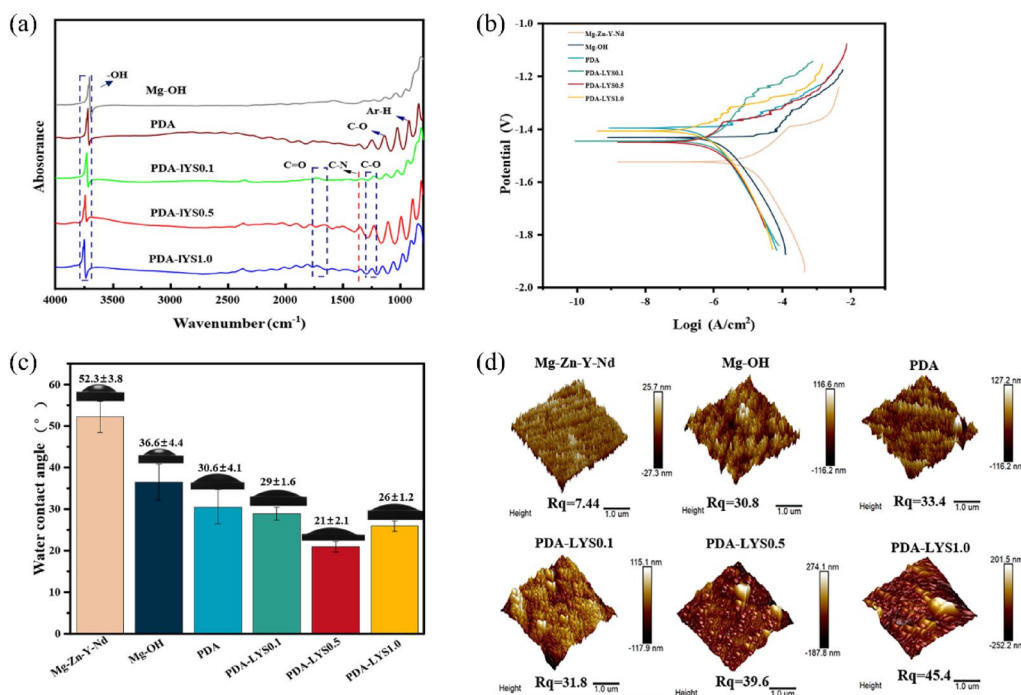
The infrared spectroscopy graphs of the samples, as illustrated in [Fig. 3(a)], revealed that the Mg-OH sample exhibited a characteristic peak of the hydroxyl groups at  $3700\text{ cm}^{-1}$ , indicating the successful preparation of Mg-OH [23]. After the self-assembly of PDA, vibration peaks of C-O bonds, C-N bonds, and Ar-H bonds were observed at  $1205\text{ cm}^{-1}$ ,  $1098\text{ cm}^{-1}$ , and  $824\text{ cm}^{-1}$ , respectively, demonstrating that PDA was successfully deposited on the alkali-heat-treated samples [12]. Upon loading the PDA-LYS coating on the samples, a new peak was observed at  $1672\text{ cm}^{-1}$ , corresponding to the stretching vibration of C=O, in addition to the stretching vibration peaks of C-N, indicating the formation of amide bonds ( $-\text{N}-\text{C}=\text{O}$ ) [24]. This provided evidence for the successful preparation of PDA-LYS on magnesium alloy.

Figure 3(b) presented the Tafel plots for various samples, and Table 1 listed the corrosion potentials and self-corrosion currents of the samples. The corrosion potential of Mg-Zn-Y-Nd sample was  $-1.52\text{ V}$ , and the corrosion current density was  $4.77 \times 10^{-6}\text{ A/cm}^2$ , the lowest corrosion potential and the highest corrosion current density among all the samples tested,

**TABLE 1:** Corrosion potential and corrosion current density of each sample.

Samples	$E_{corr}$ (V)	$I_{corr}$ ( $\text{A/cm}^2$ )
Mg-Zn-Y-Nd	-1.52	$4.77 \times 10^{-6}$
Mg-OH	-1.43	$6.71 \times 10^{-7}$
PDA	-1.39	$5.46 \times 10^{-7}$
PDA-LYS0.1	-1.44	$4.22 \times 10^{-7}$
PDA-LYS0.5	-1.44	$3.41 \times 10^{-7}$
PDA-LYS1.0	-1.47	$7.79 \times 10^{-7}$

indicating poor corrosion resistance of the bare Mg-Zn-Y-Nd alloy. The Mg-OH sample formed a uniform and dense inorganic coating, which resulted in corrosion current density of  $6.71 \times 10^{-7}\text{ A/cm}^2$ . This was an order of magnitude improvement over the corrosion current density of the magnesium alloy, demonstrating that alkali heat treatment could effectively enhance the corrosion resistance of magnesium alloy. During self-assembly, PDA oxidizes to form polydopamine, which showed a further reduced corrosion current density of  $1.57 \times 10^{-7}\text{ A/cm}^2$  compared to both Mg-Zn-Y-Nd and Mg-OH samples. This reduction was attributed to the formation of a certain thickness of polydopamine coating during the deposition process, making it difficult to penetrate during electrochemical testing. The inclusion of LYS in the PDA coating resulted in corrosion current density of  $4.22 \times 10^{-7}\text{ A/cm}^2$  for the PDA-LYS0.1 sample and  $3.41 \times 10^{-7}\text{ A/cm}^2$  for the PDA-LYS0.5 sample, indicating



**Figure 3:** (a) FTIR of coating each sample; (b) Tafel curve of each sample; (c) Water contact angle of each sample; (d) The three-dimensional morphology of different samples.

improved corrosion resistance compared to the magnesium alloy. However, it was noteworthy that the PDA-LYS1.0 sample exhibited a corrosion current density of  $7.79 \times 10^{-8}$  A/cm<sup>2</sup>, an order of magnitude reduction compared to the PDA sample, which could be related to fewer microcracks in the sample and possibly more chemical bonds formed between LYS and PDA.

As depicted in [Fig. 3(c)], Mg-Zn-Y-Nd and Mg-OH samples were measured to be  $52.3 \pm 3.8^\circ$  and  $36.6 \pm 4.4^\circ$ , respectively. The hydrophilicity of the sample was reduced due to the presence of a significant number of hydroxy groups on the hot surface of certain alkali substances. After the addition of LYS, the hydrophilicity of the coatings began to decline, and then gradually increased. This is because trace amounts of LYS are not sufficient to promote covalent cross-linking between LYS and PDA molecules, which is inhibited by excess LYS doping [18]. Therefore, the results showed that with the increase of LYS content, the water contact Angle of the samples in the PDA-LYS group increased first, then decreased and then increased.

As shown in [Fig. 3(d)], the surface of the Mg-Zn-Y-Nd sample was smooth with a low roughness of 7.44 nm, while the Mg-OH sample exhibited an Rq value of 30.8 nm, indicating an increase in roughness after the magnesium alloy's pretreatment. Upon the deposition of the PDA coating, the surface roughness of the sample further increased to 33.4 nm, which

could be attributed to increase in uneven cracks on the sample surface or the non-covalent cross-linking ( $\pi$ - $\pi$  interactions and hydrogen bonding) of PDA [25, 26]. Interestingly, with the increase in the doping ratio of LYS, the surface roughness of the samples also gradually increased, with PDA-LYS1.0 reaching the highest Rq value at 45.4 nm. This implied that the PDA-LYS1.0 sample was more conducive to cell adhesion and proliferation, thereby enhancing cell compatibility, which was beneficial for the growth of surrounding tissue cells after scaffold implantation [27].

### Hemocompatibility testing of blood

As depicted in [Fig. 4(a)], the hemolysis rate of the Mg-Zn-Y-Nd sample was the highest among all samples at 3.5%, due to the poor corrosion resistance of the magnesium alloy, which facilitated the release of high concentration of magnesium ions, leading to the rupture of red blood cells. Following this, the hemolysis rate for the PDA sample was 3.2%. Interestingly, with the increase of LYS content, the hemolysis rates of the PDA-LYS group samples decreased accordingly, with the PDA-LYS1.0 showing the lowest rate at 1.08%.

Figure 4(b) and (c) indicated that a significant amount of fibrinogen adhered to the Mg-Zn-Y-Nd sample, a consequence

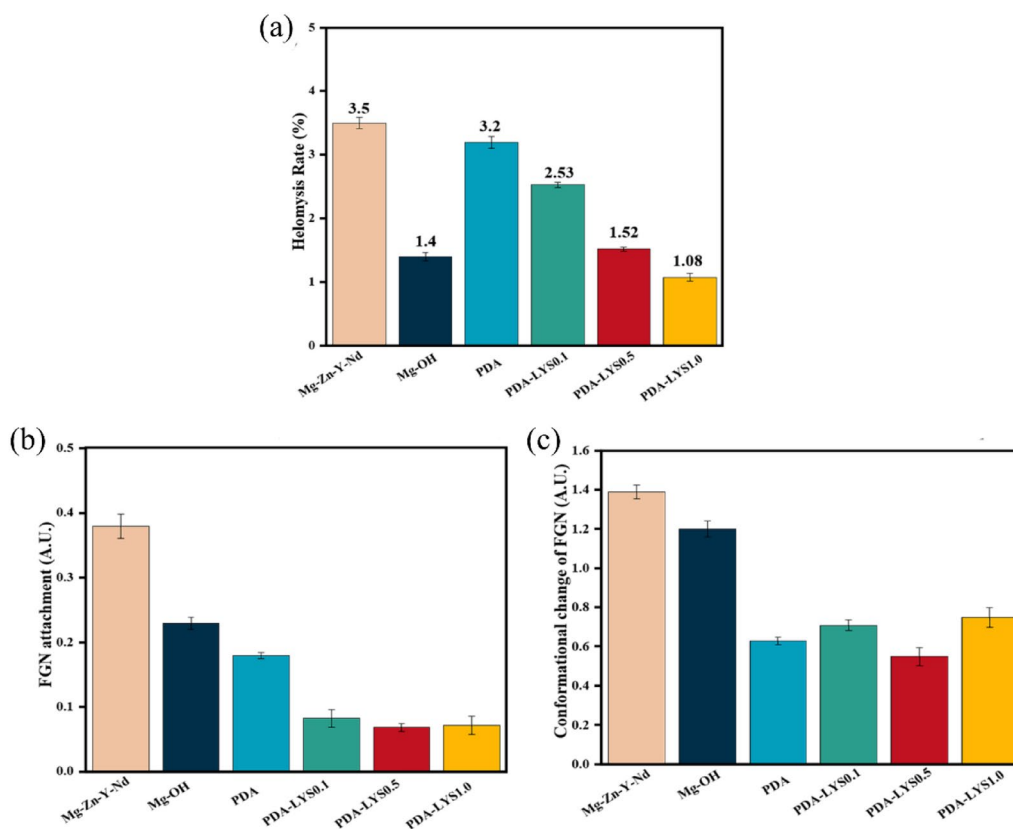


**Figure 4:** (a) The hemolysis rate of each sample; (b) Fibrinogen attachment of each sample; (c) Fibrinogen denaturation of each sample.

of the release of a large quantity of magnesium ions. Upon doping with LYS, the PDA-LYS group samples varied in their degree of reduction in fibrinogen adhesion and denaturation on the magnesium alloy, demonstrating that samples doped with LYS decreased the adhesion and denaturation of fibrinogen [28]. In summary, PDA-LYS coatings effectively enhanced the blood compatibility of magnesium alloy.

Whole blood experimental microscopic morphology analysis, as shown in [Fig. 5(a)], revealed that evident blood clots and scattered aggregations of cells with the significant presence of blood components were observed on the Mg-Zn-Y-Nd and Mg-OH samples. On the PDA sample, leukocytes were seen extending pseudopodia, indicating an activated state, suggesting that the PDA coating was likely to induce inflammation. In contrast, in the PDA-LYS group samples, the presence of red and white blood cells were extremely rare. Only a few platelets were observed, some of which were round and spherical, indicating a non-active state. This demonstrated that the PDA-LYS coating enhanced the anticoagulant ability of the magnesium alloy.

As observed in [Fig. 5(b)], a significant amount of platelets adhered to the Mg-Zn-Y-Nd, Mg-OH, and PDA samples, with considerable aggregation and extension of pseudopodia, reflecting the poor anticoagulant function of these samples. In contrast, the number of platelets on the PDA-LYS group samples

were reduced compared to the PDA, exhibiting a spherical morphology. Particularly, on the PDA-LYS0.5 and PDA-LYS1.0 samples, only a few platelets adhered in the crevices, and the platelets did not extend pseudopodia, indicating an inactive state. This reduction in platelet adhesion and maintenance of an inactive state might be attributed to the reaction between LYS and PDA, which decreased the content of positively charged amino groups on the surface of the PDA coating. In summary, the PDA-LYS coating reduced the number of platelet adhesion on magnesium alloy while maintaining the platelets in a favorable inactive state.

### Cell activity analysis and morphological analysis of endothelial cells

As depicted in [Fig. 6(a) and (b)], after 4 h of culture, most endothelial cells were observed to be in a rounded state, with minimal differences in cell viability values among the various samples. However, after 24 h of culture, a significant increase in the number of endothelial cells were noted for both PDA sample and PDA-LYS group samples, with good growth morphology, wherein the cell viability of PDA-LYS samples were significantly higher than that of other samples. Interestingly, after 72 h of culture, a pronounced declining trend in endothelial cells were observed in the Mg-Zn-Y-Nd sample, with a significant

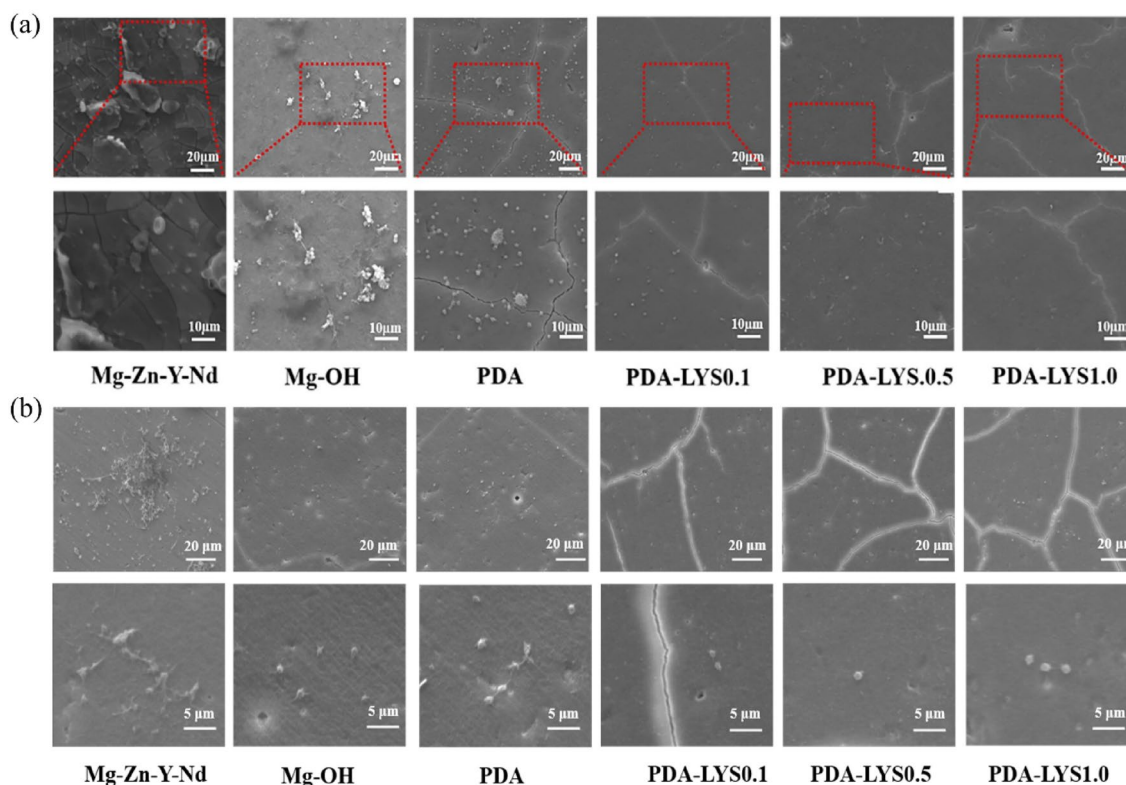


**Figure 5:** (a) Microscopic characterization images from whole blood experiments for each sample; (b) Microscopic characterization images of platelet adhesion and denaturation experiments for each sample.

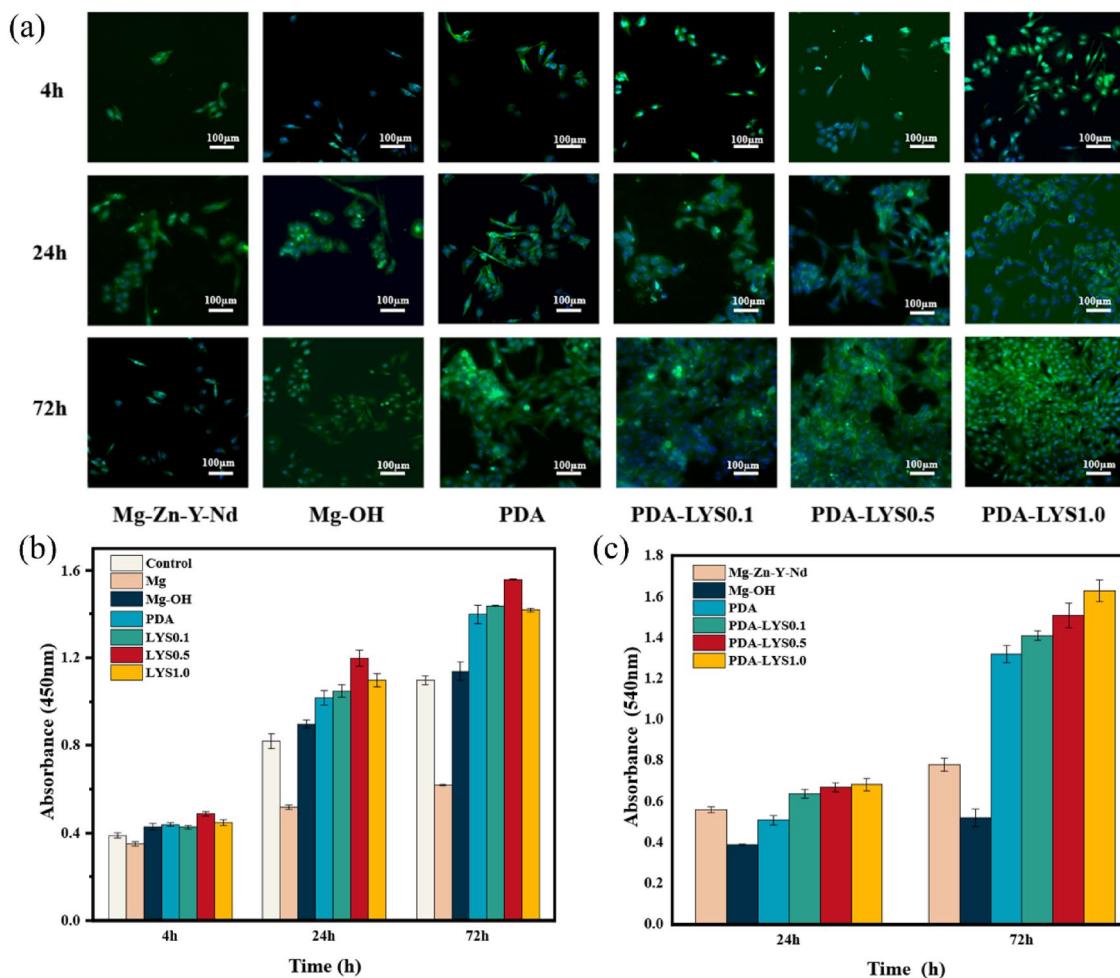


**Figure 6:** (a) The morphological images of endothelial cells at different time points in each sample; (b) The cell viability values of endothelial cells at different time points in each sample; (c) The values of nitric oxide (NO) release from endothelial cells at different time points in each sample.

increase in the number of endothelial cells cultured in the PDA-LYS group samples compared to PDA sample. These results indicate that the PDA-LYS coating positively promotes the adhesion and proliferation of endothelial cells.

### NO analysis of endothelial cells

After 4 h of endothelial cells culturing, the release of nitric oxide (NO) was minimal with little variation, thus it was not statistically evaluated. As depicted in [Fig. 6(c)], after 24 and 72 h of culturing endothelial cells, absorbance values were obtained, which were directly proportional to the NO release. Among them, the NO concentration released by endothelial cells on the surface of the Mg-Zn-Y-Nd alloy was relatively high. Considering the cell morphology, the amount of NO released was higher than expected. This was due to the poor corrosion resistance of the Mg-Zn-Y-Nd magnesium alloy, leading to the release of a large amount of  $Mg^{2+}$ , which in turn promoted the endothelial cells to release a large amount of NO [29, 30]. The

concentration of NO released on the surface of Mg-OH sample significantly decreased, indicating a reduction in magnesium ions in the extract and indirectly suggesting that the Mg-OH coating enhanced the corrosion resistance of the magnesium alloy. The NO release in the PDA-LYS group samples were notably higher; after 72 h of culture, the NO release in the PDA-LYS group samples further increased, with the PDA-LYS1.0 sample releasing the most NO. This was due to the fact that the amount of NO release was related to the number and morphology of endothelial cells, indicating that the PDA-LYS1.0 sample had a positive effect on the growth of endothelial cells.

### Apoptosis analysis of endothelial cells

As depicted in Fig. 7, after 4 h of culture, endothelial cells in the Mg-Zn-Y-Nd sample were observed to be in a shrunken state with a few dead cells, while the difference in cell numbers among other groups were not significant. After 24 h of culture, there was an increase in cell count in the PDA-LYS group samples,

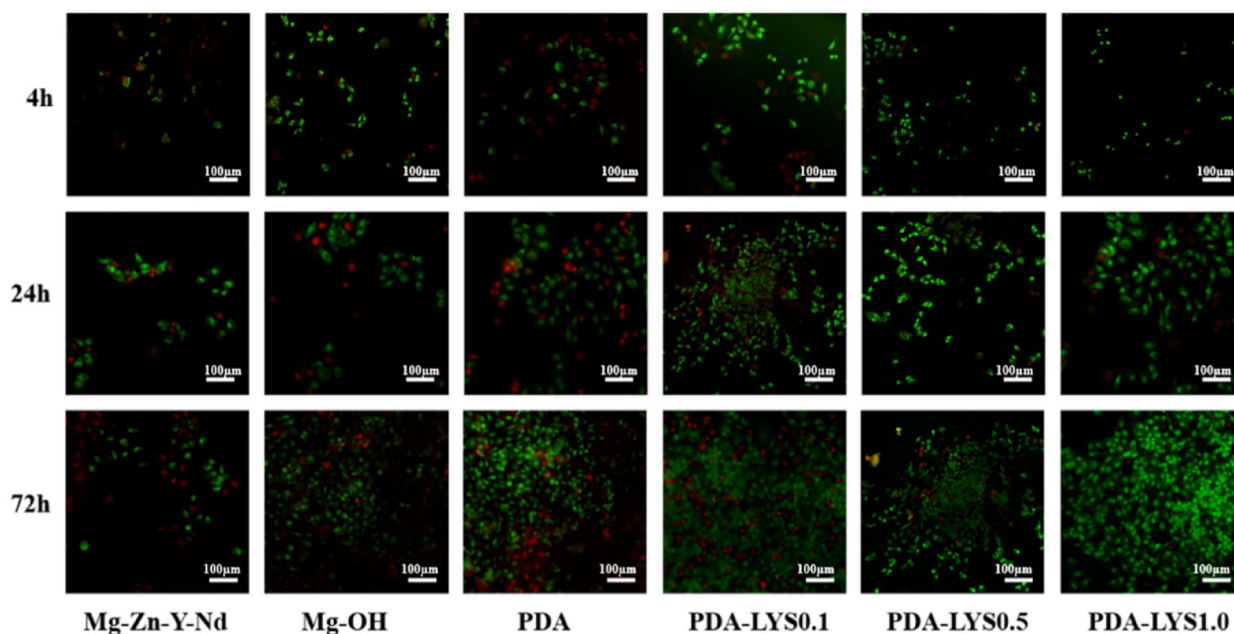


**Figure 7:** Presented fluorescence images of endothelial cell apoptosis at different time points in each sample (live cells are green, dead cells are red).

with no significant rise in the number of apoptotic cells. After 72 h of culture, compared to other groups, the PDA-LYS1.0 sample exhibited a higher cells count and a lower number of dead cells, indicating that the PDA-LYS1.0 coating had a significant positive impact on the growth of endothelial cells, creating a favorable microenvironment for endothelial cells proliferation.

### Cell activity analysis and morphological analysis of smooth muscle cells

As shown in [Fig. 8(a) and (b)], after 4 h of culture, the difference in cell viability among the samples were minimal, and the cells count of PDA sample were slightly higher. After 24 h of culture, the viability of both Mg-Zn-Y-Nd and Mg-OH samples decreased further compared to the control group, and the cell morphology was shrunken, indicating that these two groups were not conducive to the spreading and proliferation of smooth muscle cells. The viability of both PDA sample and PDA-LYS group samples were slightly higher than that of the control group cells. Notably, in the PDA-LYS0.1 sample, some cells exhibited elongated actin filaments, indicating that the sample promoted the proliferation and growth of smooth muscle cells within 24 h. After 72 h of culture, the cells viability of the PDA sample was high, with the elongated states observed, suggesting that the PDA sample facilitated the proliferation of smooth muscle cells, indicating a poorer anti-proliferative capability of PDA toward smooth muscle cells. The cell viability in the PDA-LYS group samples were below the control group, suggesting that the addition of LYS to PDA exerted a certain inhibitory effect on smooth muscle cells. Compared to 24 h,

the number of smooth muscle cells in the PDA-LYS1.0 sample changed very little, indicating that the PDA-LYS1.0 coating had a positive effect on inhibiting smooth muscle cells growth, which was beneficial to the proliferation of endothelial cells.

### Conclusion

This article demonstrated that the fabrication of the PDA-LYS composite coating on the surface of Mg-Zn-Y-Nd alloy, which effectively enhanced its endothelialization potential. Blood experiment results indicated that the magnesium alloy modified with PDA-LYS coating exhibited a lower hemolysis rate, reduced platelet adhesion and denaturation, and excellent anticoagulation capability. Cell experiments also confirmed the strong potential of this composite coating to promote endothelialization and inhibited the excessive proliferation of smooth muscle cells. Notably, the PDA-LYS1.0 sample showed good hemocompatibility and cytocompatibility. In summary, this study explored a functional composite coating that effectively improved the application potential of magnesium alloy in the cardiovascular implant field, offering new insights for the application of medical magnesium alloy.

### Materials and methods

#### Materials and coatings preparation

The Mg-Zn-Y-Nd alloy was prepared with a diameter of 10 mm and a thickness of 3 mm. The samples were initially polished using 200 to 1000-grit sandpaper and then further polished

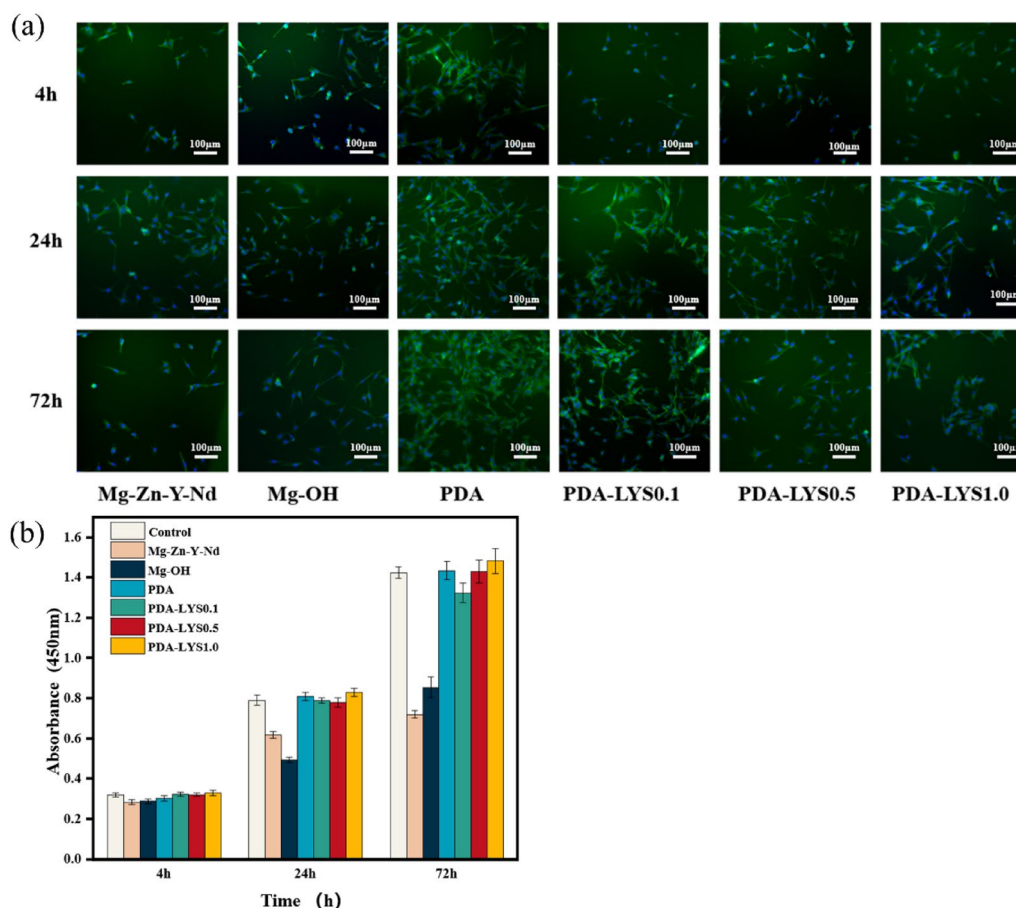


**Figure 8:** (a) The morphological images of smooth muscle cells at different time points in each sample; (b) The cell viability values of smooth muscle cells at different time points in each sample.

with a polishing machine. The processed samples were placed in absolute ethanol and sonicated for 5 min. Then, the samples were promptly soaked in a 3 M NaOH solution for 8 h at 60 °C (labeled as Mg–OH). At last, 2 mg/mL of dopamine (DA) was dissolved in HCl-Tris buffer (10 mM, pH 8.5) to prepare solutions with different DA/LYS mass ratios (1:0.1, 1:0.5, 1:1). The Mg–OH samples were then immersed in either DA or DA/LYS solutions at room temperature for 24 h. After the reaction was completed, the samples were rinsed with deionized water and subsequently dried in a desiccator. The magnesium substrates treated with DA/LYS were, respectively, named PDA, PDA-LYS0.1, PDA-LYS0.5, and PDA-LYS1.0 following the above procedure. The preparation process of the Mg–OH/PDA-LYS coatings were shown in Fig. 9.

### Surface analysis

The surface morphology of the samples were observed using a scanning electron microscope. The elemental composition of the coatings were measured using EDS energy spectrum (SEM, FEI Quanta200, The Netherlands). The composition and functional

groups of the samples were analyzed using total reflection Fourier transform infrared spectroscopy (FTIR) with a Bruker VERTEX 70V instrument from Germany. The micromorphology and roughness of the samples were measured using atomic force microscopy (AFM, Bruker/multimode, USA). The water contact angle of the samples were measured using water contact angle measuring equipment (DSA 100, Krüss, GmbH, Germany) at room temperature. The electrochemical polarization curves of various samples were measured using the RST 5200F electrochemical workstation. Prior to the test, the open-circuit voltage of the samples were measured for 10 min, followed by the Tafel curve.

### Hemocompatibility test

#### Hemolysis test

Mix fresh blood and normal saline in a ratio of 4:5 to prepare diluted blood. Then, immerse the samples to be tested in 37 °C normal saline for 30 min. Then, the diluted blood was added to normal saline and ultrapure water at 37 °C for 1 h, serving as the



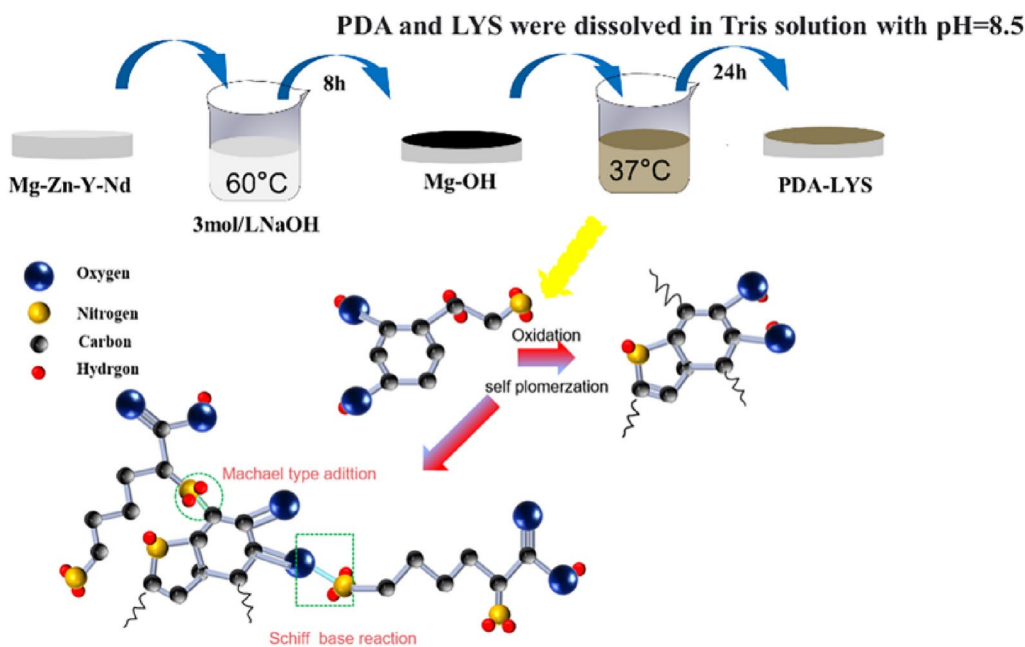


Figure 9: Coatings preparation process.

negative control group and positive control group. Finally, the solution was aspirated and centrifuged at 2500 rpm for 5 min. Finally, the absorbance at a wavelength of 540 nm was measured using an enzyme labeling instrument. The hemolysis ratio (HR) is calculated as follows:

$$HR = \frac{OD_t - OD_n}{OD_p - OD_n} \times 100\% \quad (1)$$

#### Platelet adhesion and activation; adhesion and aggregation of fibrinogen test

Fresh blood from healthy volunteers was then centrifuged in a centrifuge at 1500 r/min for 15 min to obtain a supernatant rich in plasma (PRP). After incubation, the samples were washed three times with saline. Then, they were dehydrated using a gradient of alcohol (25%, 50%, 75%, and 100%). Finally, the samples were treated with gold spray to observe the status and number of platelets adhering to them under the SEM.

The samples were placed in 24-well plates, and 6 mL of healthy adult blood was taken and centrifuged at 3000 r/min for 15 min to obtain platelet-poor plasma (PPP). 0.50 μL of PPP was then added to the surface of the samples, ensuring even distribution, and incubated at 37 °C for 60 min. After incubation, the samples were washed three times with physiological saline. Next, 50 μL of a 5% BSA blocking solution was added to cover the samples and incubated for 30 min. The samples were then washed three times with physiological saline. Subsequently, 50 μL of HRP-coupled goat anti-human fibrinogen antibody (diluted 500 times with PBS) was added

to the samples for adhesion and incubated at 37 °C. Finally, the samples were washed three times with physiological saline. After incubation, the samples were washed three times with saline. Then, 100 μL of TMB color development solution was added to the samples, and the reaction was carried out for 10 min, protected from light. Finally, 50 μL of termination solution was added to terminate the reaction. Finally, 110 μL of the solution was removed from each well and transferred to a 96-well plate. The absorbance was then measured at 450 nm using an enzyme marker.

#### Whole blood test

Fresh blood from volunteers was collected into negative pressure collection tubes containing sodium citrate. The sides and bottoms of Mg-Zn-Y-Nd, Mg-OH, PDA, and PDA-LYS samples with different parameters were sealed with silica gel. Then, 0.6 mL fresh healthy adult blood was added to the samples to be tested, and then the samples were placed in a shaker at 37 °C and 100 rpm for 1 h. After incubation, the samples were washed gently 3 times with normal saline and fixed with 4% paraformaldehyde solution for 20 min. Then the samples were rinsed with normal saline, and then dehydrated with gradient alcohol (25%, 50%, 75%, and 100%) for 10 min, respectively. After that, the finished samples were put into a drying oven to fully dry. Then the samples were sprayed with gold, and the surface morphology of the samples were observed under the electron scanning electron microscope.

## In vitro cytocompatibility test

Cell Viability Assays: Endothelial cells (ECs) and Smooth muscle cells (SMCs) viability were assessed via CCK-8 solution after incubation in coated and uncoated samples. Apoptosis Experiments: Used AO/EB staining to determine the coatings' effects on endothelial cell apoptosis. Nitric Oxide (NO) release assay from endothelial cells. Morphological Characterization: The growth and morphology of ECs and SMCs on various coatings were observed using laser confocal microscopy after specific staining protocols.

## Acknowledgments

This research was funded by National Nature Science Foundation of China (No. U2004164 and 51671175).

## Author contributions

Yi Ma: Conceptualization, Methodology, Validation Formal analysis, Data Curation, Writing—original draft, Writing—review & editing. Hao-jie Guo: Conceptualization, Methodology, Data Curation. Jing-an Li: Supervision, Resources. Yan-chao Wang: Formal analysis. Yi fan Zhou: Funding acquisition, Project administration, Resources.

## Funding

This study was funded by National Nature Science Foundation of China, No. U2004164, 51671175.

## Data availability

The data presented in this study are available on request from the authors.

## Declarations

**Conflict of interest** The authors declare that they have no known competing financial interests or personal relationships that could have appeared to influence the work reported in this paper.

## Supplementary Information

The online version contains supplementary material available at <https://doi.org/10.1557/s43578-024-01386-6>.

## References

- Z.Z. Sheng, X. Liu, L.L. Min, H.L. Wang, W. Liu, M. Wang, L.Z. Huang, F. Wu, X. Hou, *Chin. Chem. Lett.* **28**(6), 1131 (2017). <https://doi.org/10.1016/j.ccl.2017.03.033>
- J. Canfield, H. Totary-Jain, *J. Pers. Med.* (2018). <https://doi.org/10.3390/jpm8040033>
- K. Kumar, R.S. Gill, U. Batra, *Mater. Technol.* **33**(2), 153 (2017). <https://doi.org/10.1080/10667857.2017.1377973>
- R.A. Byrne, M. Joner, A. Kastrati, *Eur. Heart J.* **36**(47), 3320 (2015). <https://doi.org/10.1093/eurheartj/ehv511>
- M. Chagnon, L.G. Guy, N. Jackson, *Toxicol. Pathol.* **47**(3), 390 (2019). <https://doi.org/10.1177/0192623318816936>
- J.L. Niu, H. Huang, J. Pei, Z.H. Jin, S.K. Guan, G.Y. Yuan, *Biomater. Transl.* **2**(3), 236–247 (2021). <https://doi.org/10.12336/biomatertransl.2021.03.06>
- Y. Chen, T. Ying, Y. Yang, J. Wang, X. Zeng, *Corros. Sci.* (2023). <https://doi.org/10.1016/j.corsci.2023.111106>
- R. Motallebi, Z. Savaedi, H. Mirzadeh, *J. Mater.* **20**, 1873 (2022). <https://doi.org/10.1016/j.jmrt.2022.07.154>
- Z.Q. Zhang, Y.X. Yang, J.A. Li, R.C. Zeng, S.K. Guan, *Bioact. Mater.* **6**(12), 4729 (2021). <https://doi.org/10.1016/j.bioactmat.2021.04.044>
- B. Wang, S.K. Guan, J. Wang, L.G. Wang, S.J. Zhu, *Mater. Sci. Eng. B* **176**(20), 1673 (2011). <https://doi.org/10.1016/j.mseb.2011.03.015>
- L.Y. Li, L.Y. Cui, R.C. Zeng, S.Q. Li, X.B. Chen, Y. Zheng, M.B. Kannan, *Acta Biomater.* **79**, 23 (2018). <https://doi.org/10.1016/j.actbio.2018.08.030>
- Z.J. Han, H.J. Guo, Y.F. Zhou, L.G. Wang, K. Zhang, J.A. Li, *Metals.* (2022). <https://doi.org/10.3390/met12040545>
- L.C. Zhang, M.Z. Xu, Y.D. Hu, F. Gao, T. Gong, T. Liu, X. Li, C.J. Pan, *Appl. Surf. Sci.* **451**, 20 (2018). <https://doi.org/10.1016/j.apsusc.2018.04.235>
- X.L. Liu, Z. Zhen, J. Liu, T.F. Xi, Y.D. Zheng, S.K. Guan, Y.F. Zheng, Y. Cheng, *J. Mater. Sci. Technol.* **31**(7), 733 (2015). <https://doi.org/10.1016/j.jmst.2015.02.002>
- T. Mohd, Y.C. Ma, M.J. Xu, Q. Wang, Y.H. Lin, X.W. Kong, *Ind. Eng. Chem. Res.* **59**(45), 19840 (2020). <https://doi.org/10.1021/acs.iecr.0c03368>
- J. Li, T.S. Li, Y.W. Zeng, C.C. Chen, H.L. Guo, B. Lei, P. Zhang, Z.Y. Feng, G.Z. Meng, *Colloid Surf.* (2023). <https://doi.org/10.1016/j.colsurfa.2022.130361>
- X.J. Cui, X.Z. Lin, C.H. Liu, R.S. Yang, X.W. Zheng, M. Gong, *Corros. Sci.* **90**, 402 (2015). <https://doi.org/10.1016/j.corsci.2014.10.041>
- A. Barrantes, J. Wengenrotha, T. Arnebrant, H.J. Haugena, *J. Colloid Interface Sci.* **485**, 288–295 (2017). <https://doi.org/10.1016/j.jcis.2016.09.046>
- N. Gallo, S. Quarta, M. Massaro, M.A. Carluccio, A. Barca, D. Cannoletta, L. Siculella, L. Salvatore, A. Sannino, *Pharmaceutics* (2023). <https://doi.org/10.3390/pharmaceutics15020479>
- Y. Li, C. Liang, L. Gao, S.Y. Li, Y.Z. Zhang, J. Zhang, Y. Cao, *Mater. Chem. Front.* **1**(12), 2664 (2017). <https://doi.org/10.1039/c7qm00402h>

21. T. Liu, Z. Zeng, Y. Liu, J. Wang, M.F. Maitz, Y. Wang, S.H. Liu, J.Y. Chen, N. Huang, ACS Appl. Mater. **6**(11), 8729 (2014). <https://doi.org/10.1021/am5015309>
22. Y.Q. Zhang, J. Man, J.N. Liu, J.Y. Li, X.Z. Song, J.L. Wang, J.F. Li, Y.G. Chen, ACS Appl. Mater. **15**(23), 27719 (2023). <https://doi.org/10.1021/acsami.3c05077>
23. Y.X. Wu, L. Chang, J.A. Li, L.G. Wang, S.K. Guan, J. Biomater. Appl. **35**(2), 158 (2020). <https://doi.org/10.1177/0885328220926655>
24. B.C. Yi, L. Yu, H. Tang, W.B. Wang, W. Liu, Y.Z. Zhang, Appl. Mater. Today (2021). <https://doi.org/10.1016/j.apmt.2021.101198>
25. Y.C. Huang, T. Zhu, Z.J. Zhu, H.X. Yuan, L.R. Tan, P.P. Yao, Y.N. Qiao, C.Z. Zhu, J. Xu, ACS Appl. Polym. Mater. **5**(7), 5707 (2023). <https://doi.org/10.1021/acsapm.3c00983>
26. R.N. Zhang, Y.L. Su, X.T. Zhao, Y.F. Li, J.J. Zhao, Z.Y. Jiang, J. Membr. Sci. **470**, 9 (2014). <https://doi.org/10.1016/j.memsci.2014.07.006>
27. G.E. Salvi, N.P. Lang, Biol. Med. **12**(3), 262 (2001). <https://doi.org/10.1177/10454411010120030501>
28. N. Sahiner, Polymer **121**, 46 (2017). <https://doi.org/10.1016/j.polymer.2017.06.014>
29. M. Liu, X. Wang, B. Sun, H. Wang, X. Mo, M. El-Newehy, M.M. Abdulhameed, H. Yao, C. Liang, J. Wu, Int. J. Biol. Macromol. **259**(2), 129283 (2024). <https://doi.org/10.1016/j.ijbiomac.2024.129283>
30. J.A. Maier, Acta Physiol. **240**(3), 14110 (2024). <https://doi.org/10.1111/apha.14110>

**Publisher's Note** Springer Nature remains neutral with regard to jurisdictional claims in published maps and institutional affiliations.

Springer Nature or its licensor (e.g. a society or other partner) holds exclusive rights to this article under a publishing agreement with the author(s) or other rightsholder(s); author self-archiving of the accepted manuscript version of this article is solely governed by the terms of such publishing agreement and applicable law.